

# Efficient Nearest Neighbor Search Using Dynamic Programming

Pengfei Wang, Jiantao Song, Shiqing Xin (Corresponding author), Shuangmin Chen, Changhe Tu, Wenping Wang, Jiaye Wang

**Abstract**—When dealing with point clouds distributed on manifold surfaces in 3D space, or when the query point is far from the data, the efficiency of traditional nearest neighbor search algorithms (e.g., KD Tree and R Tree) may degrade. In extreme cases, the complexity of the query can approach  $O(n)$ . In this paper, we propose a novel dynamic programming technique that precomputes a Directed Acyclic Graph (DAG) to enable more efficient nearest neighbor queries for 2D manifold data. By leveraging this structure, only a small number of distance comparisons between point pairs are required to accurately identify the nearest neighbor. Extensive experimental results demonstrate that our method achieves query speeds that are 1x-10x faster than traditional methods. Moreover, our algorithm exhibits significant potential. It achieves query efficiency comparable to KD-trees on uniformly distributed point clouds. Additionally, our algorithm supports nearest neighbor queries among the first  $k$  points. Coupled with our algorithm, a farthest point sampling algorithm with lower complexity can also be implemented. Furthermore, our method has the potential to support nearest neighbor queries with different types of primitives and distance metrics. We believe that the method proposed in this paper represents the most concise and straightforward exact nearest neighbor search algorithm currently available, and it will contribute significantly to advancements in the field.

**Index Terms**—Nearest neighbor search, farthest point sampling, density peak clustering, delaunay, voronoi diagram.

## I. INTRODUCTION

**G**IVEN a target point set  $\mathcal{P} = \{p_i\}_{i=1}^n$  and a query point  $q$ , the point  $p_i$  is considered the nearest neighbor in  $\mathcal{P}$  to  $q$  if  $p_i$  satisfies

$$\forall j \in [1, n], \|q - p_i\| \leq \|q - p_j\| \quad (1)$$

where  $\|\cdot\|$  denotes the Euclidean distance. Finding the nearest neighbor is a fundamental operation in various fields, including computer graphics [1]–[3], computer vision [4], [5], and robotics [6]. Due to its critical applications in various fields, improving query speed is an ongoing pursuit. Traditional nearest-point query methods include KD Tree [7], R Tree [8], all of which offer fast nearest-neighbor query speeds for general point clouds. These methods achieve rapid query speeds by constructing hierarchical structures to partition the space or point cloud, allowing for quick localization during the query phase. However, when dealing with data distributed along 2D manifold surfaces embedded in 3D space (referred to as 2D manifold data), which are commonly encountered in the field of computer graphics, or when the query point is distant from the given data, the query efficiency of traditional algorithms may decrease. In some cases, the query complexity could degrade to  $O(n)$ .

As shown in the inset figure, we have two point clouds with distinct distributions: one uniformly distributed within a unit cube, and the other distributed across the surface of the Earth. Additionally,

we generate two sets of query points—one within the bounding box of the input data, and the other within 8x the bounding box. It can be observed that the query performance of both KD Tree and R Tree significantly degrades under these conditions.

In this paper, we present a simple, effective, and novel nearest point query algorithm based on Voronoi / Delaunay. For 2D manifold data in 3D, our query speed is 1x-10x faster than KD Tree and R Tree. Even for uniformly distributed random point clouds, our query algorithm achieves speeds comparable to KD Tree. Our main contributions are as follows:

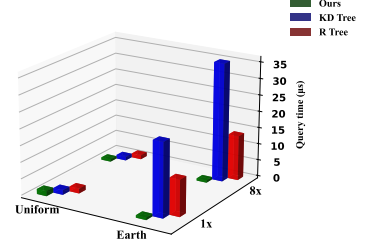
- We introduced a concise nearest neighbor search algorithm for 2D manifold point cloud data that significantly improves query speed compared to traditional algorithms.
- If the point cloud possesses an order, our method can facilitate the identification of the nearest point to  $q$  among  $\{p_i\}_{i=1}^m$ , for any  $m$ , where  $m < n$ . This approach can be employed to reduce the time complexity of Density Peak Clustering [9], thus enhancing its applicability in large-scale scenarios.
- Based on our method, we developed a farthest point sampling algorithm with an average complexity of  $O(k \log n)$  in 3D, where  $n$  represents the total number of points and  $k$  denotes the number of samples.

Additionally, our algorithm exhibits significant potential. For instance, under various primitive types and distance metrics, as long as the incremental Voronoi or Delaunay construction algorithms for the primitives, as well as the distance query function from a point in space to the primitive, are provided, our nearest neighbor search framework can support nearest neighbor searches in these contexts. However, further development will be necessary in future work.

## II. RELATED WORK

### A. Exact Nearest Neighbor Search

For spatial data, the nearest neighbor problem is usually solved by building a spatial index [10]. These indices can broadly be divided into two categories: those that partition the space and those that partition the data.



Classic structures for space partitioning include KD Tree and quadtrees. A KD Tree [7] is a spatial partitioning structure that recursively divides the dataset along one of the  $k$  coordinate system axes, typically alternating between them; for instance, with  $k = 2$ , splits occur alternately on the  $x$ - and  $y$ -axes. This splitting process continues until a maximum depth is reached or until fewer than a specified number of points remain in a cell. KD Trees can be extended to include objects beyond points, such as triangles or line segments. Determining the optimal splitting plane can be challenging in these cases; However, for points (or disks) in two dimensions, we can simply sort the points along each dimension and split at the median. The construction of a KD Tree can be achieved in  $O(n \log n)$  time, and it can find the nearest neighbors in  $O(\log n)$  time. A octree is another spatial partitioning structure, but it specifically divides a 3D space into eight cubes or regions. This is typically done recursively, with each subdivision occurring when the data within a region meets certain criteria, such as exceeding a maximum number of points or objects. Each internal node in the octree corresponds to a cube region of space, which is further subdivided into eight equal-sized cubes, represented by its children. The construction of an octree can be completed in  $O(n \log n)$  time, and it can find the nearest neighbors in  $O(\log n)$  time, too.

The R Tree [8] is a classic structure for partitioning data. It is based on B-trees and shares a similar structure: both the number of objects in a leaf node and the number of children in an internal node are bounded by specified minimum and maximum limits. Additionally, all leaf nodes are at the same level. The R-tree can be built in  $O(n \log n)$  time and allows for the identification of the nearest neighbors in  $O(\log n)$  time.

Grids and linear search methods are also classic approaches for nearest-neighbor searches. The grid-based approach improves efficiency by overlaying a regular grid on the entire simulation area and tracking the agents within each cell. During a query, the search includes the cell containing the query points and the adjacent cells. The construction time for this method is  $O(n + m)$ , where  $m$  represents the number of cells in the grid. The worst-case query time is  $O(n)$ , but practical performance greatly depends on the distribution of agents and the size of the cells. On the other hand, linear search is suitable when the number of query points is very small. This method finds the nearest points by calculating the distance from each target point to the query point.

### B. Voronoi Diagram & Delaunay

Suppose that we have a set of generators  $\mathcal{S} = \{s_i\}_{i=1}^n$  in a given domain  $\Omega$  that is equipped with a metric function  $\mathcal{D}$ , the Voronoi diagram involves partitioning  $\Omega$  into regions such that the generator  $s_i$  dominates a region

$$\text{Cell}(s_i) = \{x \in \Omega \mid \mathcal{D}(s_i, x) \leq \mathcal{D}(s_j, x), j \neq i\}. \quad (2)$$

The definition of Voronoi diagrams may vary with domains, metrics, and generator types. The most prevalent version assumes that  $\Omega$  represents Euclidean spaces, and the generators are exclusively points. As a fundamental tool, this has found widespread applications in computer graphics [1], [3], [11].

The Delaunay is the dual structure of the Voronoi diagram, representing the adjacency relationships between the Voronoi cells. Currently, Voronoi diagrams are typically computed by first calculating the Delaunay triangulation and then deriving the dual structure. The Watson algorithm [12] is a classic method for computing the Delaunay triangulation. It is based on the empty circle property and works by incrementally inserting points and flipping triangles that do not satisfy this property. Common tools for computing Delaunay include TetGen [13] and CGAL [14], which can achieve an average computational complexity of  $O(n \log n)$ , with a worst-case complexity of  $O(n^2)$ .

Voronoi diagrams can also be applied to nearest neighbor searches. By definition, if the closest point to a query point  $q$  in  $\mathbf{P}$  is  $p_k$ , then  $q$  lies within the Voronoi cell of  $p_k$ . This property makes Voronoi diagrams highly relevant for solving nearest neighbor problems. However, the challenge lies in efficiently identifying the specific Voronoi cell containing  $q$ , as there currently isn't an efficient algorithm for this task. This limitation restricts the practical use of Voronoi diagrams in nearest neighbor searches.

### C. Farthest Point Sampling

Farthest point sampling (FPS) is a technique widely employed in computational geometry and computer graphics applications. It is designed to iteratively select points from a dataset such that each newly selected point is maximally distant from the previously chosen points. This method can be formally expressed as follows:

$$p_{i+1} = \arg \max_{p \in P} \left( \min_{p_j \in S} d(p, p_j) \right), \quad (3)$$

where:

- $P$  represents the set of points in the point cloud,
- $S$  denotes the subset of points that have already been selected,
- $d(p, p_j)$  is the distance between points  $p$  and  $p_j$ ,
- $p_{i+1}$  is the next point selected such that its minimum distance to any point in  $S$  is maximized.

This sampling strategy ensures that the selected points are well-distributed, making it effective for approximating shapes, surfaces, or distributions. FPS is particularly useful in applications requiring a representative subset of data points, such as mesh generation, surface simplification, or cluster initialization.

However, a notable drawback of FPS is its computational cost. The complexity of the method is  $O(kn)$ , where  $n$  is the total number of points in the dataset, and  $k$  denotes the number of points to be sampled. This complexity can become prohibitive for large datasets or when a high number of samples is needed, making FPS less efficient in such cases.

## III. METHODOLOGY

In this section, we introduce the key concept underlying the algorithms discussed in this paper, beginning with an exploration of linear search.

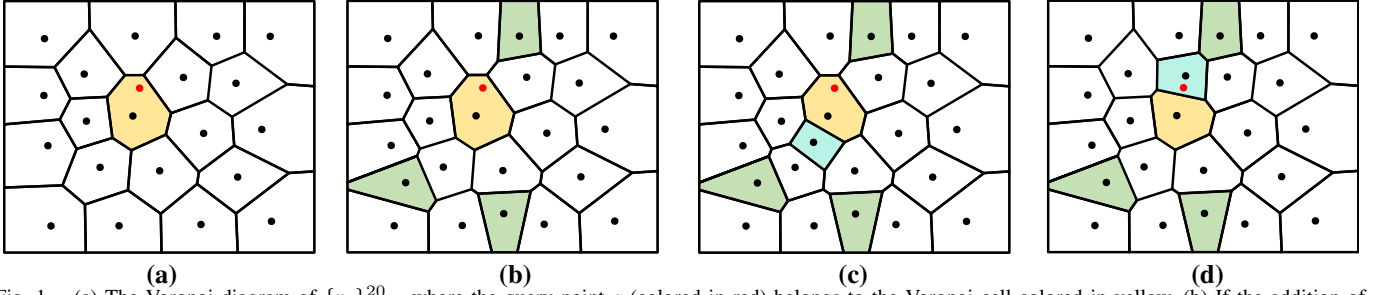


Fig. 1. (a) The Voronoi diagram of  $\{p_i\}_{i=1}^{20}$ , where the query point  $q$  (colored in red) belongs to the Voronoi cell colored in yellow. (b) If the addition of the three sites (whose cells are colored in green) does not change the yellow cell,  $\Phi_m(q)$  remains unchanged when  $m$  is increased from 20 to 23. (c) When the 24-th site  $p_{24}$  is added (see the cyan cell), the yellow cell diminishes; yet  $\Phi_{24}(q) = \Phi_{23}(q)$  if  $q$  is nearer to the old site. (d)  $\Phi_{24}(q) = p_{24}$  if  $q$  is nearer to the newly added site  $p_{24}$ .

We assume that the given points are numbered from 1 to  $n$ . Given a query point  $q$ , we use  $\Phi_m(q)$  to denote the closest point in  $\{p_i\}_{i=1}^m$ , where  $m \leq n$ . This leads to the following state transfer equation:

$$\Phi_m(q) = \begin{cases} p_1 & \text{if } m = 1, \\ \Phi_{m-1}(q) & \text{if } m \neq 1 \text{ \& } \|q - \Phi_{m-1}(q)\| \leq \|q - p_m\|, \\ p_m & \text{if } m \neq 1 \text{ \& } \|q - \Phi_{m-1}(q)\| > \|q - p_m\|, \end{cases} \quad (4)$$

which can be understood as a dynamic programming problem, where  $\Phi_n(q)$  is the actual nearest point to be extracted. Obviously, a naïve implementation of the query operation costs  $O(n)$  time. In the following, we consider how to boost this implementation.

Recall that Voronoi diagrams [15] precisely characterize how the space of interest is divided by the given data points. A point  $q$  is nearest to  $p_i$  if and only if  $q$  is located in  $p_i$ 's cell. However, Voronoi diagrams are not well-suited for NNS due to their lack of hierarchical representation. Despite this, during the incremental construction process of Voronoi Diagram, the area dominated by a site either remains unchanged or shrinks, encoding the history of how the proximity structure changes when a new point is added. Let the input point cloud be  $\mathcal{P} = \{p_i\}_{i=1}^n$ . We illustrate our construction process by considering any moment of constructing the Voronoi diagram through incremental point insertion, such as  $\mathcal{V}_m$ , which is constructed from the set  $\{p_i\}_{i=1}^m$ , where  $m \leq n$ .

Figure 1(a) shows the Voronoi diagram  $\mathcal{V}_{20}$  determined by 20 sites, with one of the cells highlighted in yellow. By adding three additional sites (whose cells are highlighted in green), we obtain a new Voronoi diagram  $\mathcal{V}_{23}$ ; see Figure 1(b). It can be seen that the addition of the three green sites does not change the yellow cell. Therefore, if  $q$  is located in the yellow cell, then  $\Phi_{23}(q) = \Phi_{20}(q)$ , implying that the nearest site to  $q$  remains unchanged even when the three green sites are added. Only when a newly added site changes the yellow cell may the nearest site differ. Specifically,  $\Phi_{24}(q) = \Phi_{23}(q)$  if  $q$  is nearer to the old site (see Figure 1(c)), and  $\Phi_{24}(q) = p_{24}$  if  $q$  is nearer to the new site  $p_{24}$  (see Figure 1(d)). To summarize, by using  $p_{m+1} \not\vdash \text{Cell}(\Phi_m(q); \mathcal{V}_m)$  to represent that the addition of  $p_{m+1}$  does not diminish the cell of  $\Phi_m(q)$  in  $\mathcal{V}_m$ , we have:

$$p_{m+1} \not\vdash \text{Cell}(\Phi_m(q); \mathcal{V}_m) \quad \mapsto \quad \Phi_{m+1}(q) = \Phi_m(q), \quad (5)$$

or

$$\begin{aligned} p_{m+j} \not\vdash \text{Cell}(\Phi_m(q); \mathcal{V}_{m+j-1}), \quad \forall 1 \leq j \leq k \\ \downarrow \\ \Phi_{m+k}(q) = \Phi_{m+k-1}(q) = \dots = \Phi_m(q). \end{aligned} \quad (6)$$

#### IV. ALGORITHM

##### A. Query Table Construction

Based on Section III, we can design a data structure called the Query Table, denoted as  $\mathcal{L} = \{\mathcal{L}_i\}_{i=1}^n$ , to store the necessary information for the query phase. Specifically, we assign each point  $p_i$  a corresponding vector  $\mathcal{L}_i$ , called Query List. During the incremental construction of the Voronoi diagram, when  $p_j$  is inserted, if the condition  $p_j \vdash \text{Cell}(p_i; \mathcal{V}_{j-1})$  is satisfied, we push  $p_j$  to the end of  $\mathcal{L}_i$ .

Query Table  $\mathcal{L}$  is constructed synchronously as the Voronoi diagram is incrementally built. Initially, we have only one site  $p_1$ , leaving its Query List empty. Suppose that the addition of  $p_{m+1}$  changes  $p_i$ 's cell in  $\mathcal{V}_m$ . We append  $p_{m+1}$  to  $p_i$ 's Query List; see Figure 2. The Query Table  $\mathcal{L}$  is completed once all the sites are inserted. It is important to note that the order of elements stored in each  $\mathcal{L}_i$  are consistent with the insertion order.

Since the Delaunay is the dual of the Voronoi diagram and reflects the adjacency relationships between Voronoi cells, to check whether  $p_m \vdash \text{Cell}(p_i; \mathcal{V}_{m-1})$ , this can be further converted into checking whether  $p_m$  and  $p_i$  are adjacent in the Delaunay constructed from  $\{p_i\}_{i=1}^m$ , which is dual to  $\mathcal{V}_m$ . Algorithm 1 provides the pseudocode for the corresponding construction process.

##### B. Nearest Neighbor Query

In the query phase, we initialize the nearest site as  $p_1$ , which implies  $\Phi_1(q) = p_1$ . Let  $p_2$  be the first site in  $p_1$ 's Query List  $\mathcal{L}_1$ , and we visit  $\mathcal{L}_1$  in order. If  $p_2$  provides a smaller distance than  $p_1$ , we switch to  $p_2$ 's Query List  $\mathcal{L}_2$ . Otherwise, we move to the next site in  $\mathcal{L}_1$  to see if it can provide a smaller distance. See the rightmost figure of Figure 2 for how the query algorithm operates. See Algorithm 2 for the pseudocode of the query algorithm.

##### C. Farthest Point Sampling

Sections IV-A and IV-B describe the algorithm for constructing the Query Table and performing nearest neighbor

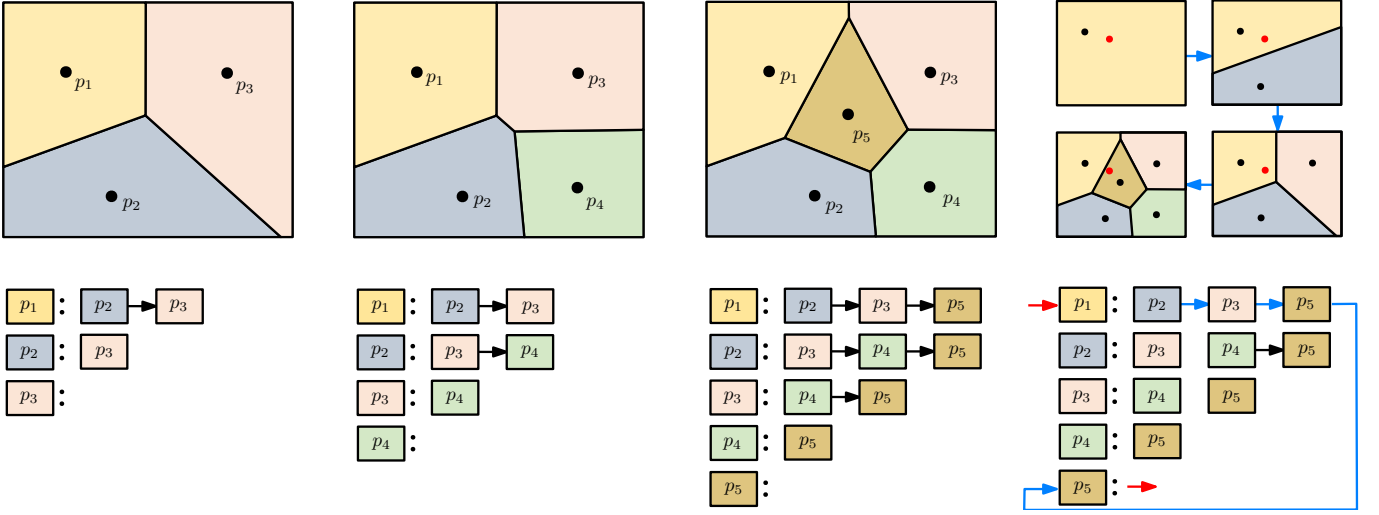


Fig. 2. We consider an incremental construction process of the Voronoi diagram of  $\{p_i\}_{i=1}^n$ . During the process, we append  $p_j$  to  $p_i$ 's Query List if the addition of  $p_j$  changes  $p_i$ 's cell. The rightmost figure shows the query process.

---

**Algorithm 1: Query Table Construction**


---

**Input:** Point cloud  $\mathcal{P} = \{p_i\}_{i=1}^n$ .  
**Output:** Query Table  $\{\mathcal{L}_i\}_{i=1}^n$ .  
Initialize the Query Table  $\mathcal{L} = \{\mathcal{L}_i\}_{i=1}^n$ .  
Insert  $p_1$ , initialize the Delaunay structure  $\mathbf{D}$ .  
**foreach**  $i$  in  $[2, n]$  **do**  
    Initialize the set  $\omega$  as empty.  
    Insert  $p_i$  and update  $\mathbf{D}$ .  
    Extract all points adjacent to  $p_i$ , store them in  $\omega$ .  
    **foreach**  $p_x$  in  $\omega$  **do**  
        Push  $p_i$  to the back of  $\mathcal{L}_x$ .  
    **end**  
**end**

---



---

**Algorithm 2: Nearest Neighbor Search**


---

**Input:** Query Table  $\{\mathcal{L}_i\}_{i=1}^n$  and query point  $q$ .  
**Output:** The closest point to  $q$ .  
getNearestNeighbor( $p_I = p_1$ )  
**foreach**  $p$  in  $\mathcal{L}_I$  **do**  
    **if**  $\|q - p\| < \|q - p_I\|$  **then**  
        **return** getNearestNeighbor( $p$ )  
    **end**  
**end**  
**return**  $p_I$

---

searches. The algorithm assumes a specific order of the point cloud and incrementally constructs the Voronoi / Delaunay based on this order. When the point cloud is unordered or there is no need to compute the nearest point to  $q$  among the first  $n$  points, we can sort the points in a specific manner to enhance the efficiency of the query phase.

Intuitively, the more uniformly the inserted point cloud is distributed in space, the faster the query speed. This is because it facilitates a transition from large to small spatial jumps during the query process. Farthest point sampling, a commonly used downsampling method, aims to distribute the

sampled points as uniformly as possible across the point cloud. Drawing inspiration from this, we set the number of sampled points equal to the total number of points in the cloud and use the sampling order to incrementally construct the Voronoi diagram. Notably, by integrating this approach into our construction process, we developed a farthest point sampling strategy with reduced complexity, leading to faster sampling times.

An important step in the farthest point sampling process involves calculating the distance between the newly sampled point and all remaining points, followed by updating the distance information. However, in most cases, the distances for the majority of the remaining points do not require updating, leading to a significant waste of computational resources. By integrating this process with our construction method, we can optimize the calculations by updating the distances for only a small subset of remaining points that are likely to change. This approach improves the algorithm's efficiency.

As an example, consider a state from the incremental construction of the Voronoi diagram, as shown in Figure 3(a). The black points represent the points that have already been inserted, while the gray points denote the remaining points waiting to be inserted. When a new point is inserted based on the farthest point sampling strategy, as illustrated in Figure 3(b), the red point represents the newly sampled point from the gray points, and the green area corresponds to its Voronoi cell. A key observation is that only the distances of the remaining points located within the cells adjacent to the green cell (specifically, those within these cells prior to the insertion of the red point) need to be updated. Since the white Voronoi cell does not change during the insertion of new points, this implies that the nearest neighbors of the uninserted points within it remain unchanged. This significantly reduces the computational cost of sampling. The remaining task is to dynamically track the Voronoi cells that contain the remaining points as the Voronoi diagram is incrementally constructed. This process is straightforward.

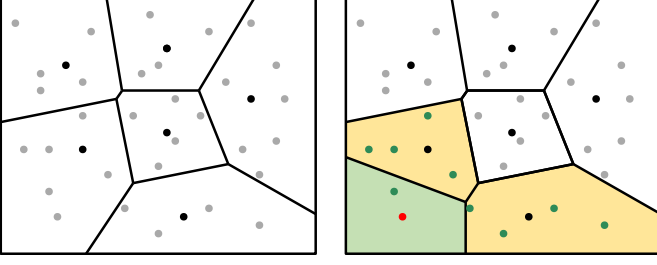


Fig. 3. Coupling of Farthest Point sorting with incremental Voronoi Construction. Left: Uninserted points (gray) are distributed within the Voronoi cells of the inserted points (black). Right: When a new point is inserted, only the distance of the uninserted points within the green and yellow cells may need to be updated.

#### D. Complexity Analysis

In this section, we will analyze the complexity of the farthest point sampling as a standalone component, rather than as part of the construction phase.

**Time Complexity of Query Table Construction.** The complexity of the Query Table Construction is the same as that of the incremental Delaunay construction. On average, the time complexity for constructing a Delaunay in 3D is  $O(n \log n)$ , while the worst-case time complexity is  $O(n^2)$ . However, this worst-case scenario is seldom encountered in typical construction processes.

**Space Complexity of the Query Table.** On average, the number of neighbors for a Voronoi cell in 3D is a constant, denoted as  $c$ . This implies that when a new point is inserted, it is adjacent to  $c$  cells on average, requiring the point to be appended to the end of  $c$  Query Lists. Therefore, the average space complexity of the Query Table is

$$O\left(\sum_{i=2}^n c\right) = c * O(n) = O(n), \quad (7)$$

where  $n$  is the number of points.

**Time Complexity of Nearest Neighbor Query.** When querying the nearest neighbor for the point  $q$ , the complexity of the query phase depends on the number of times the cell containing  $q$  (which may change during the query process) shrinks during the incremental construction, as a comparison is needed each time the Voronoi cell containing  $q$  shrinks. Simply put, assuming  $\Phi_m(q)$  is known and a new point  $p_{m+1}$  is inserted, the cell of  $p_{m+1}$  typically adjacent to  $c$  cells on average. Therefore, the probability that  $\text{Cell}(\Phi_m(q); \mathcal{V}_m)$  shrinks is approximate  $c/m$ , indicating the possibility of needing a comparison. Thus, the average time complexity of the nearest neighbor query phase is

$$O\left(\sum_{i=1}^{n-1} \frac{c}{i}\right) = c * O(\log n) = O(\log n). \quad (8)$$

**Time Complexity of Farthest Point Sampling.** When we have already inserted  $k$  points to construct the Voronoi diagram, each cell, on average, contains  $(n - k)/k$  remaining points. Given the distances from all remaining points to the nearest sampled points are known, selecting the next point for sampling has a complexity of  $O(\log(n - k))$ . Knowing that

the newly inserted point is adjacent to  $c$  cells, the number of remaining points that potentially need their distances updated is  $c \times (n - k)/k$ .

Thus, the additional complexity caused by the farthest point sampling process is:

$$O\left(\sum_{k=1}^{n-1} \left[ \log(n - k) + \left( c * \frac{n - k}{k} \right) \right] \right) \quad (9)$$

$$= O\left(\sum_{k=1}^{n-1} \log(k) + c * n * \sum_{k=1}^{n-1} \frac{1}{k} - (n - 1) * c\right) \quad (10)$$

$$= O(n \log n) \quad (11)$$

## V. RESULTS

**Hardware environment.** Our algorithm was implemented in C++ on a platform featuring a 3.4 GHz AMD Ryzen 9 5950X 16-Core CPU, 64GB of RAM, and running the Windows 11 operating system.

**Experimental parameters.** We utilized CGAL [14] for Delaunay computations. In our experiments, we used random sorting and farthest point sorting as insertion order. We measured and recorded both the construction performance and query performance for each method. The space for randomly generating query points was confined within the bounding box with 8x the volume (with edge lengths twice that of the original bounding box) of the input point cloud. The number of query points generated was set at 1000K.

**Relevant approaches for comparison.** Currently, there are numerous algorithms [16]–[19] available for nearest neighbor search. In this paper, we selected two of the fastest and most classic methods for comparison.

- 1) KD Tree: We utilized the implementation from the nanoflann library [20], setting the maximum number of leaf nodes to 10. According to tests referenced in [21], this implementation is currently the fastest for nearest neighbor searches.
- 2) R Tree: We used the implementation from Boost Library [22].

In all the experiments below, Ours<sup>1</sup> refers to our method using a random order for incremental Delaunay construction, while Ours<sup>2</sup> indicates that the farthest point sorting strategy was applied. All the point cloud data used in the experiment has been included in the supplementary data.

#### A. Query Table

*a) Length of the query list for a vertex:* Recall that the Query Table maintains a list of points encroached upon during the incremental construction of the Delaunay for each vertex in  $V$ . It is evident that the Voronoi cells of points inserted earlier often shrink more times, resulting in longer Query Lists. Therefore, to investigate how the length of the Query List varies with different insertion indexes, we conducted a study using the 100K-vertex dragon point cloud as an example. As shown in Figure 4, we have plotted the length of the query list for each point with respect to its insertion order. Although the impact of random sorting and farthest point



TABLE I  
THE AVERAGE (AVG) AND VARIANCE (VAR) OF THE LENGTH OF THE QUERY LIST AND THE NUMBER OF COMPARISONS REQUIRED PER QUERY ON CLASSICAL MODELS.

		Camel	Bunny	Dragon	Kitten	Armadillo	Lucy	Sponza
Vertices		28934	72911	100313	291023	726367	1018219	1313504
Ours <sup>1</sup>	Avg	15.913	15.805	15.684	15.397	15.832	16.034	14.631
	Var	17.911	17.264	17.705	18.834	17.631	17.968	20.431
	Tested	171.783	166.726	209.516	182.719	234.742	276.549	418.285
Ours <sup>2</sup>	Avg	14.414	14.345	14.165	13.964	14.370	14.478	13.067
	Var	16.783	15.906	16.491	17.126	16.172	16.584	19.681
	Tested	144.754	135.831	161.822	155.806	197.042	235.085	358.413

sorting strategies on the length of the Query List is not readily apparent from the figure, we calculated the average lengths of the Query Lists to be 15.684 and 14.165, with standard deviations of 17.705 and 16.491, respectively. The farthest point sorting resulted in a shorter and more uniform distribution of the Query List. Similar results were obtained across multiple data. This characteristic enables the query table generated through farthest point sorting to facilitate faster nearest-neighbor searches.

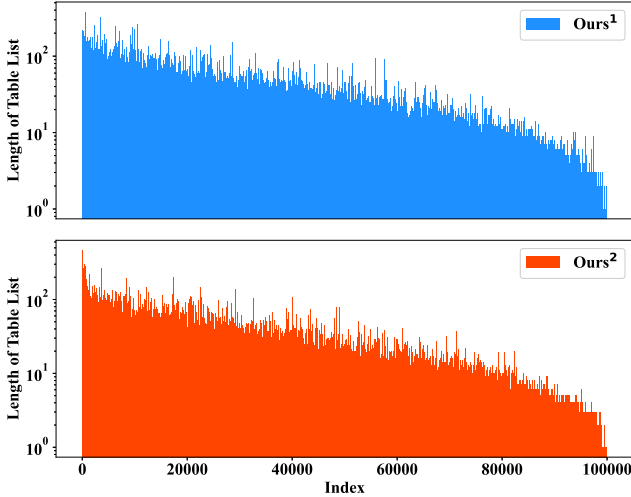


Fig. 4. The length of the Query List for different index points. Top: random sorting. Bottom: farthest point sorting.

b) *Number of tested vertices:* As shown in Algorithm 2, the nearest neighbor search problem is transformed into the task of calculating distances between points.

The number of distance comparisons between points during the query process partially reflects the efficiency of the nearest neighbor search. We tested several classical models and recorded the number of comparisons, along with the mean and variance of the Query Lists, as shown in Table I. It can be observed that, after utilizing the farthest point sorting method, both the average length (Avg) and variance (Var) of the Query Lists decreased, accompanied by a reduction in the average number of comparisons during the nearest neighbor search process.

TABLE II  
PREPROCESSING TIME (s) ON CLASSICAL MODELS.

	Camel	Bunny	Dragon	Kitten	Armadillo	Lucy	Sponza
Vertices	28934	72911	100313	291023	726367	1018219	1313504
KD-tree	0.004	0.011	0.016	0.051	0.149	0.215	0.281
R-tree	0.005	0.014	0.022	0.062	0.170	0.243	0.311
Ours <sup>1</sup>	1.097	3.205	4.692	14.46	41.58	62.13	72.31
Ours <sup>2</sup>	1.876	5.818	8.473	35.64	96.11	263.3	307.6

### B. Preprocessing Cost

When a random sorting method is adopted, the preprocessing time of the current algorithm is equivalent to that of incremental Delaunay construction. However, at this stage, our preprocessing speed is slower than that of existing Delaunay construction libraries. This is primarily due to two factors. First, our method currently supports only serial execution. Second, certain algorithms, such as TetGen, reorder points before incremental Delaunay construction to enhance overall speed. However, this insertion order is not favorable for our queries. It is worth noting, however, that our method has the potential to accelerate preprocessing when integrated with Delaunay construction. In the current implementation, we present the preprocessing times of different algorithms across several classic models in Table II. Additionally, Figure 5 shows the preprocessing time with respect to the resolution of the Dragon data, comparing our method to other methods. It can be observed that at this stage, the preprocessing time of our method exceeds that of existing nearest neighbor search algorithms.

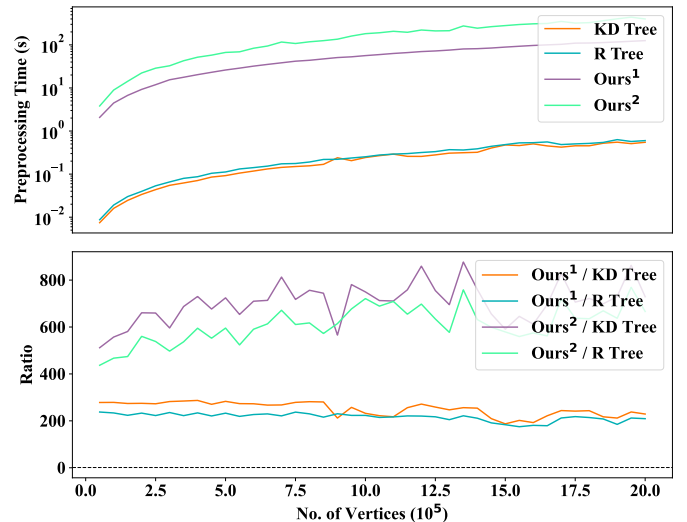


Fig. 5. The preprocessing cost of KD Tree, R Tree and Ours on the Dragon data with varying resolutions. Top: preprocessing time. Bottom: the comparison about the preprocessing cost. Dashed line indicates where the ratio equals 1.

### C. Query Performance

Using the Dragon dataset as an example, we present the query cost of our method compared to other approaches with

respect to resolution in Figure 6, demonstrating the significant advantage of our method in this scenario. In Table III, we provide more detailed examples for several classical models.

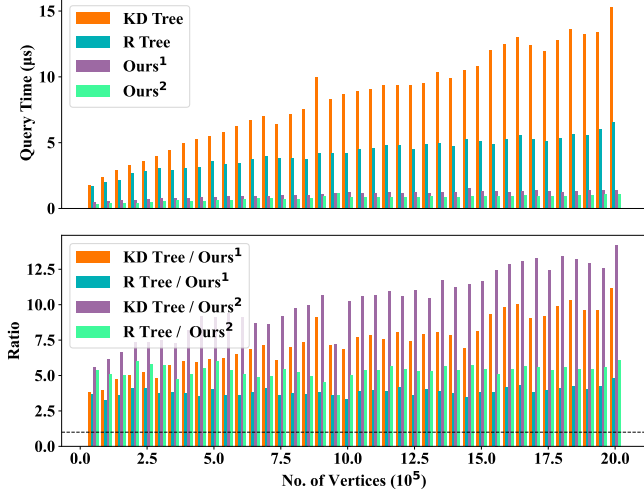


Fig. 6. Average query time on the Dragon model with varying resolutions. Top: Average query time ( $\mu s$ ) among KD tree, R tree and ours. Bottom: The comparison about the average time different methods. Dashed line indicates where the ratio equals 1.

TABLE III  
AVERAGE QUERY TIME ( $\mu s$ ) OF KD TREE, R TREE, AND OURS ON CLASSICAL MODELS. THE **HIGHEST** AND **SECOND-FASTEST** QUERY TIMES ARE HIGHLIGHTED IN BOLD AND UNDERLINED, RESPECTIVELY.

	Camel	Bunny	Dragon	Kitten	Armadillo	Lucy	Sponza
Vertices	28934	72911	100313	291023	726367	1018219	1313504
KD Tree	1.639	3.795	2.475	8.475	12.81	9.796	4.407
R Tree	1.623	2.739	2.034	5.359	5.241	4.518	<u>1.851</u>
Ours¹	<u>0.423</u>	<u>0.559</u>	<u>0.540</u>	<u>0.957</u>	<u>1.132</u>	<u>1.293</u>	2.146
Ours²	<b>0.344</b>	<b>0.482</b>	<b>0.388</b>	<b>0.752</b>	<b>0.834</b>	<b>1.070</b>	<b>1.694</b>

#### D. Tests on ABC & Thingi10K

Thingi10K [23] and ABC [24] are two large-scale 3D datasets that contain diverse models. To conduct a comprehensive comparison among KD Tree, R Tree, and Ours, we ran them on the dataset to compare both the preprocessing cost and the query cost. The query time are shown in Figures 7 and Figure 8. And the preprocessing time can be found in Figure 13 and Figure 14 in Appendix.

#### E. Other Types of Data

a) *Uniform Point Cloud.*: To fully demonstrate the efficiency of the algorithm, we compared KD Tree, R Tree, and Ours on uniform point clouds. As shown in Figure 9, it can be observed that even on completely uniform point clouds, our method remains comparable in query efficiency to the fastest current implementation of KD Tree and R Tree.

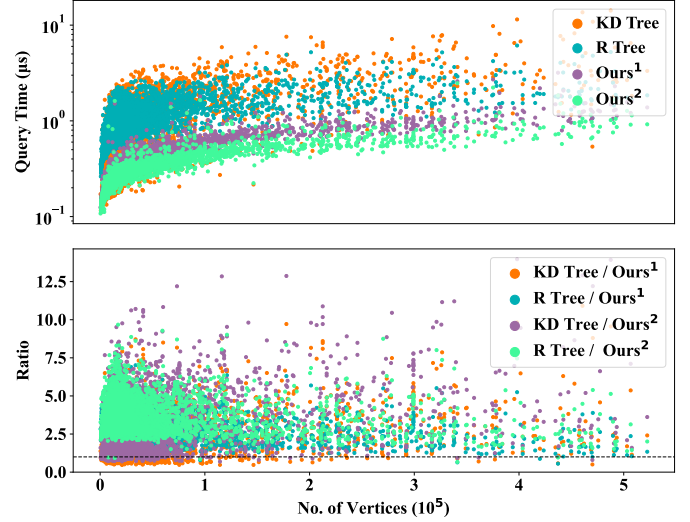


Fig. 7. Comparison about query performance on ABC dataset. Top: the average timing cost per query ( $\mu s$ ) for KD Tree, R Tree and Ours. The y-axis is scaled logarithmically. Bottom: the comparison about the query cost among KD Tree, R Tree and Ours. Dashed line indicates where the ratio equals 1.

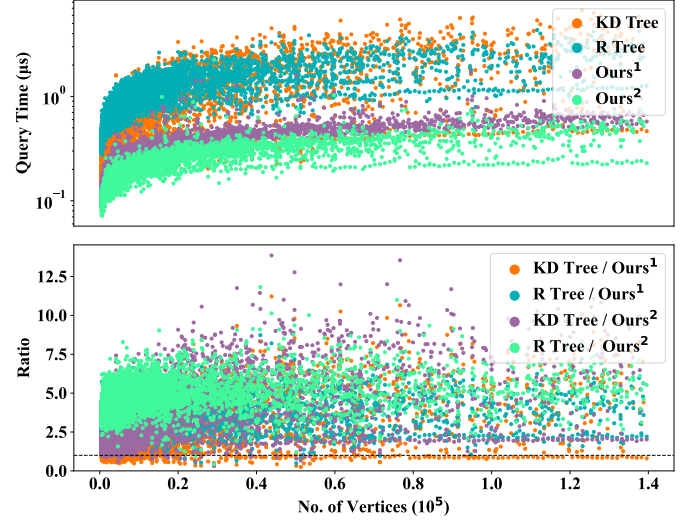


Fig. 8. Comparison about query performance on Thingi10K data. Top: the average timing cost per query ( $\mu s$ ) for KD Tree, R Tree and Ours. The y-axis is scaled logarithmically. Bottom: the comparison about the query cost among KD Tree, R Tree and Ours. Dashed line indicates where the ratio equals 1.

b) *Earth City.*: Additionally, we tested the efficiency of the KD Tree, R Tree, and our method on an Earth data, distributed over a sphere, with the results shown in Figure 10. At this distribution, both KD Tree and R Tree exhibit a significant drop in efficiency. However, our method remains extremely fast, achieving up to 40x the query speed of KD Tree.

#### F. Near and far query points.

Additionally, we observed that the location of query points at different positions can impact the efficiency of the query. To further investigate this, we conducted tests on uniformly distributed point clouds, point clouds representing Earth cities, and the Dragon model, with the number of points in each point cloud controlled at 1,000K. The results are presented in Figure 11. The horizontal axis represents the ratio of the length

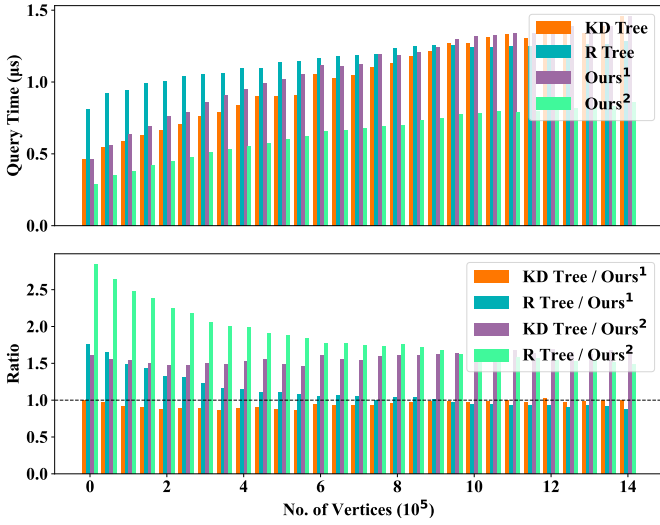


Fig. 9. Average query time on the uniform point cloud with varying resolutions. Top: Average query time per query ( $\mu s$ ) among KD Tree, R Tree and Ours. Bottom: The comparison of the average time of different methods. Dashed line indicates where the ratio equals 1.

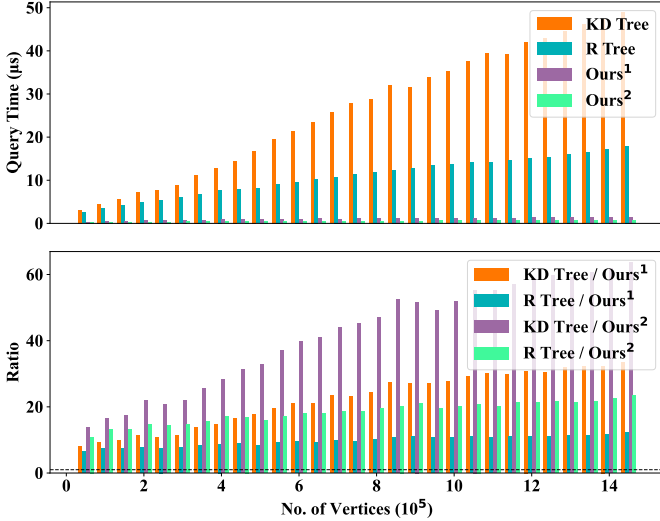


Fig. 10. Average query time on the earth data with varying resolutions. Top: Average query time among KD tree, R tree and ours. Bottom: The comparison about the average time different methods. Dashed line indicates where the ratio equals 1.

of the generation space for the query points to the length of the bounding box of the target points along any coordinate axis. It can be observed that even in a completely uniform point cloud distribution, where the query point generation space matches the bounding box of the target points, our query speed remains comparable to that of the KD Tree. In other scenarios, our method demonstrates a significant advantage in query speed.

## VI. DESIRABLE PROPERTIES

Beyond its speed advantages, we believe the current method holds significant potential, and future high-quality research could further expand the algorithm's capabilities. In the following section, we will analyze several key aspects.

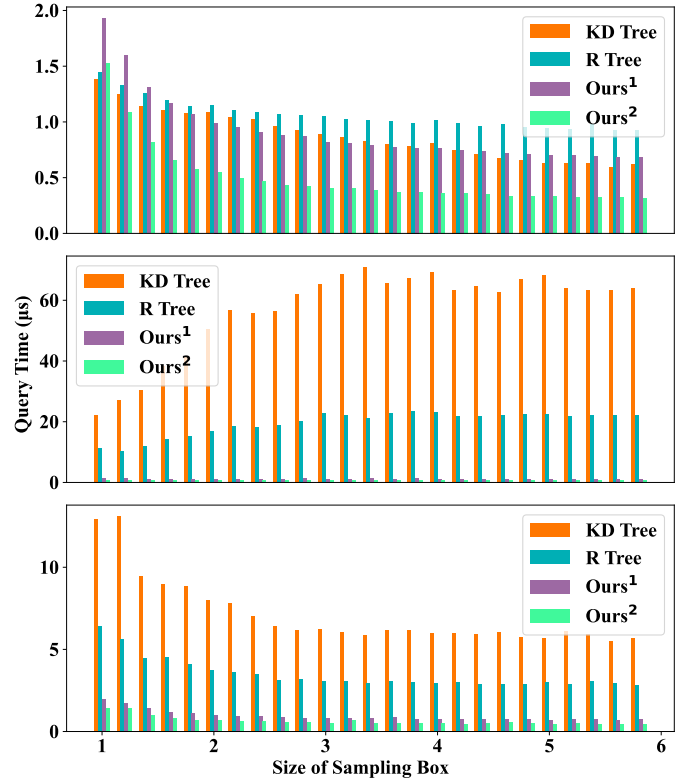


Fig. 11. Average query time with varying sizes of the sampling box (arbitrary axis ratio, with volume ratio calculated as the cube of the axis ratio). Top: Uniform point cloud. Middle: Earth city data. Bottom: Dragon point cloud.

### A. Nearest Neighbor Among the First $n$ Points

One notable property of our algorithm is that, given any query point  $q$  and integer  $k$ , we can efficiently identify the nearest point among  $\{p_i\}_{i=1}^k, k \leq n$ . Specifically, the order of the given points is used to incrementally construct the Delaunay. As discussed in Section III, during the nearest-neighbor search process, when querying the nearest neighbor, we only need to compute  $\Phi_n(q)$ . However, in practice,  $\forall i \in [1, n]$ ,  $\Phi_i(q)$  is already incorporated into our query process. When a specific  $k$  is provided, as shown in Algorithm 2, our query process can terminate early. To the best of our knowledge, no existing algorithm is capable of achieving this.

The Density Peak Clustering algorithm [9] is a well-known method for clustering. One critical step in this algorithm is the calculation of  $\sigma_i$ , which is defined as:

$$\delta_i = \min_{j: \rho_j > \rho_i} (d_{ij}), \quad (12)$$

$\rho_i$  is defined as the density of point  $p_i$ , and  $d_{ij}$  represents the distance between points  $p_i$  and  $p_j$ . Generally, computing  $\{\delta_i\}_{i=1}^n$  requires calculating the distance between every pair of points, which has a complexity of  $O(n^2)$ . However, for 3D points, using our algorithm, this problem can be solved in  $O(n \log n)$  time.

### B. Farthest Point Sampling.

Farthest Point Sampling (FPS) is a widely used sampling algorithm due to its ability to ensure uniform sampling of points, making it broadly applicable. For instance, in the



PointNet++ [25] framework for 3D point cloud deep learning, FPS is employed to sample and cluster points as part of the receptive field. The complexity of sampling  $k$  points from  $n$  points is  $O(kn)$ . Currently, there are approximate farthest point sampling algorithms designed for specific types of point clouds [26], but as far as we know, no breakthroughs have been made in reducing the complexity of exact farthest point sampling. However, based on our algorithm, we achieve a complexity of  $O(k \log n)$  for sampling  $k$  points from  $n$  points in 3D space.

### C. Various Primitives & Distance Metrics

Many existing nearest neighbor search algorithms are designed for specific types of primitives and distance metrics, which limits their generalizability across diverse scenarios. In contrast, our method, as described in Sections III, IV-A, and IV-B, requires only the incremental construction of the Voronoi diagram for the primitives and a distance query function from any point in space to the primitives, making it straightforward to integrate into our nearest neighbor query framework. For instance, by supplying only the algorithm for incrementally constructing the Voronoi diagram of triangles under the Manhattan distance, along with a function to query the Manhattan distance between a spatial point and a triangle, our framework can efficiently determine the nearest primitive to a given point under the Manhattan distance. We believe this is a significant advantage of our algorithm. Of course, we acknowledge that the incremental construction of Voronoi diagrams for various primitives is quite challenging; however, as outlined below, we also provide alternative options.

### D. Fast Preprocessing & Slow Query

We acknowledge that the preprocessing efficiency of our algorithm is relatively low, especially in high-dimensional spaces. Furthermore, as previously mentioned, the incremental construction of Voronoi diagrams for various primitives under different distance metrics presents significant challenges. Therefore, we propose a new direction. As discussed in Section IV-A, when constructing the Query Table, we need to identify the set  $\omega_m$  upon the insertion of  $p_m$ , as shown in Algorithm 1. The set is defined as follows:

$$\omega_m = \{p_i \mid p_m \vdash \text{Cell}(p_i; \mathcal{V}_{m-1})\}. \quad (13)$$

In fact, when dealing with complex high-dimensional or intricate scenarios, computing  $\omega_m$  becomes extremely challenging. Therefore, we compute  $\omega_m^*$  instead, which only needs to satisfy  $\omega \subseteq \omega_m^*$ , while still ensuring accurate nearest neighbor results. This approach offers a direction for performing fast nearest neighbor searches in high-dimensional spaces and scenarios involving different primitives and distance metrics. As a result, the computed set may contain redundancies, leading to a slight reduction in the speed of the nearest neighbor search. Additionally, we believe that even if  $\omega_m$  does not belong to  $\omega_m^*$ , it could provide valuable insights for developing approximate nearest neighbor search algorithms.

### E. Fast Query & Slow Preprocessing

Another encouraging finding is that the number of comparisons in our query process, as shown in Table I, can be further reduced, suggesting potential for additional algorithmic acceleration. Specifically, as previously outlined in our algorithm, when we focus on the time point  $\Phi_k(q) = p_k$  during the query process, the current approach only utilizes the information that  $q \in \text{Cell}(\Phi_k(q); \mathcal{V}_k)$ . However, we can infer that  $q \in \cap_{\Phi_i(q)=p_i, 1 \leq i \leq k} \text{Cell}(\Phi_{i-1}(q); \mathcal{V}_{i-1}) \cap \text{Cell}(\Phi_k(q); \mathcal{V}_k)$  from the query process.

As illustrated in Figure 12, (a) and (b) depict a simple incremental construction process, with the red dot representing the query point  $q$ . In this example, we have only utilized the information shown in (c), namely that  $q \in \text{Cell}(p_3; \mathcal{V}_3)$ . As shown in brown in (c). However, based on the query process, we can infer that  $q \in \text{Cell}(p_1; \mathcal{V}_2) \cap \text{Cell}(p_3; \mathcal{V}_3)$ . As shown in (d). This enables us to design a more rigorous and precise occupancy evaluation. Our method currently does not leverage this information during the query process, even though it can be obtained through complex preprocessing, which would, of course, involve substantial preprocessing overhead.

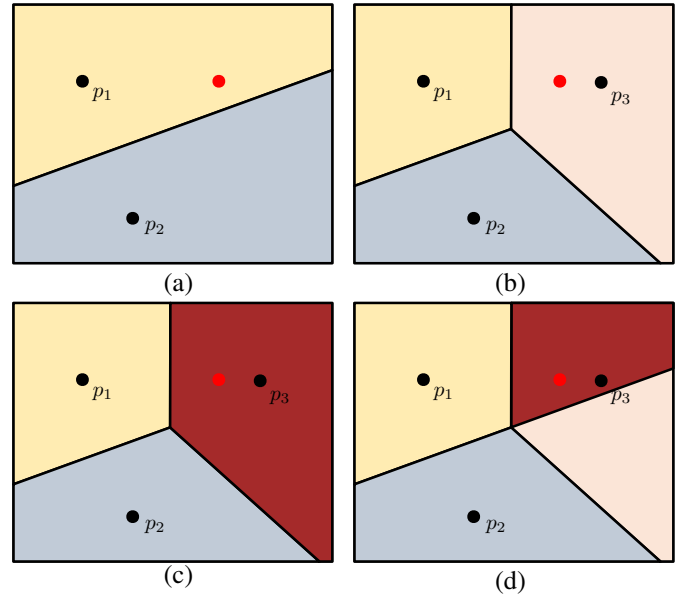


Fig. 12. (a) and (d): A simple incremental insertion process, with the red dot representing the query point  $q$ . (c) Based on the query process of (a)(b), we know the information  $q \in \text{Cell}(p_3; \mathcal{V}_3)$ , as shown in brown. (d) In fact, the complete information we can obtain is  $q \in \text{Cell}(p_1; \mathcal{V}_2) \cap \text{Cell}(p_3; \mathcal{V}_3)$ , as shown in brown.

However, we also recognize that utilizing all of the aforementioned information would result in significantly increased preprocessing complexity. To balance this, we implemented a simplified approach that compromises between the algorithm described in this paper and the information mentioned in this section. In brief, in addition to  $q \in \text{Cell}(p_i; \mathcal{V}_i)$ , we incorporated  $q \in \text{Cell}(\Phi_{i-1}; \mathcal{V}_{i-1}) \cap \text{Cell}(p_i; \mathcal{V}_i)$ . This region is used as the fundamental unit for occupancy evaluation, rather than a complete Voronoi cell.

We were pleasantly surprised to find that, despite implementing only a simplified version, we achieved a significant reduction in the number of comparisons compared to Table I. As shown in Table IV,  $Ours_1^*$  and  $Ours_2^*$  represent the

TABLE IV  
THE NUMBER OF PAIRWISE COMPARISONS DURING THE QUERY PROCESS  
USING DIFFERENT CONSTRUCTION STRATEGIES.

	Camel	Bunny	Dragon	Kitten	Armadillo	Lucy	Sponza
Vertices	28934	72911	100313	291023	726367	1018219	1313504
Ours <sup>1</sup>	171.783	166.726	209.516	182.719	234.742	276.549	418.285
Ours <sup>2</sup>	144.754	135.831	161.822	155.806	197.042	235.085	358.413
Ours <sup>1</sup> <sub>*</sub>	93.218	97.49	108.545	107.708	127.760	134.123	124.615
Ours <sup>2</sup> <sub>*</sub>	75.453	74.055	88.089	82.812	94.953	106.269	124.547

number of comparisons without and with farthest point sampling, respectively, under the strategy outlined in this section. Remarkably, only around 100 pairwise distance comparisons are required to find the exact nearest neighbor for a query point among 1 million points. However, we must acknowledge that while the number of comparisons has decreased, the actual query time has increased. We speculate that this may be due to increased memory usage by the data structure during the query phase, which likely results in more cache misses, thereby reducing efficiency. Nevertheless, we believe this is a highly meaningful direction for further exploration.

## VII. LIMITATIONS AND FUTURE WORK

The main drawback of our algorithm at present is its preprocessing cost, which limits its application in some scenarios. However, fortunately, our method supports nearest neighbor queries during the construction process, which may assist in the tetrahedron location problem during incremental Delaunay construction, offering a potential avenue for accelerating preprocessing. Therefore, in future work, we will focus on improving the preprocessing speed. Additionally, our method currently only supports nearest neighbor search; we aim to extend the current algorithm to support k-nearest neighbor queries in the future. Furthermore, all the properties mentioned in Section VI are goals we aim to address in our future work.

## VIII. CONCLUSION

In this paper, we observe that when dealing with point clouds distributed over 2D manifolds in 3D space, or when query points are distant from the target points, the efficiency of traditional nearest neighbor search algorithms decreases. In certain special cases, the complexity can degrade to  $O(n)$ . Inspired by the incremental Delaunay construction process, we propose a nearest neighbor search algorithm specifically for 2D manifold point cloud. Our method achieves 1-10 times the speed of KD Tree in nearest neighbor searches. We validated the efficiency advantages of our approach through extensive experiments.

Additionally, our algorithm demonstrates significant potential. For instance, it supports querying the closest point to  $q$  among any of the first  $k$  points. This capability facilitates the application of peak clustering algorithms to large-scale data scenarios. Moreover, we have implemented a farthest point

sampling algorithm with  $O(k \log n)$  complexity in 3D space. Our method can efficiently identify the point closest to the query point from a set of 1 million points by performing about 100 pairwise distance comparisons.

We believe that the algorithm presented in this paper holds significant potential for application and will make a substantial contribution to the community.

## APPENDIX

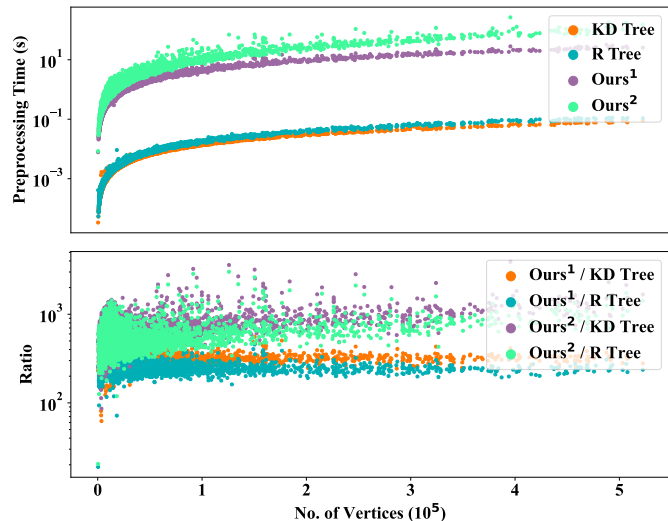


Fig. 13. Comparison about preprocessing cost on ABC dataset. Top: the time cost of preprocessing for KD Tree, R Tree and ours. Bottom: the comparison about the preprocessing cost among KD Tree, R Tree and ours.

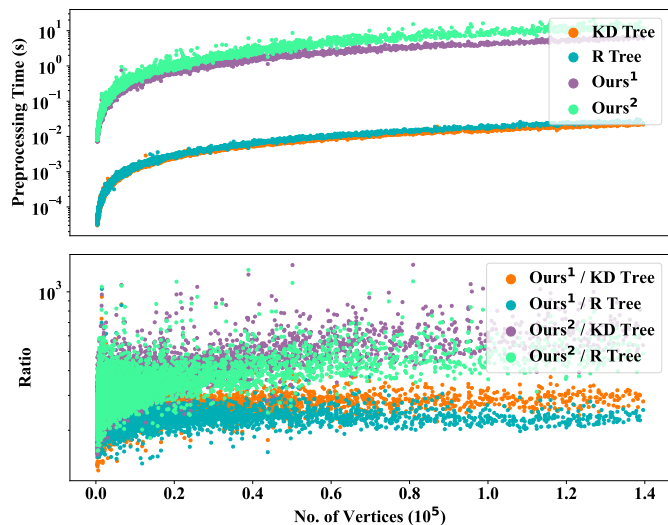


Fig. 14. Comparison about preprocessing cost on Thing10K dataset. Top: the time cost of preprocessing for KD Tree, R Tree and ours. Bottom: the comparison about the preprocessing cost among KD Tree, R Tree and ours.

## REFERENCES

- [1] R. Xu, Z. Wang, Z. Dou, C. Zong, S. Xin, M. Jiang, T. Ju, and C. Tu, "Rfeps: Reconstructing feature-line equipped polygonal surface," *ACM Transactions on Graphics (TOG)*, 2022.
- [2] K. Pearson, "Liii. on lines and planes of closest fit to systems of points in space," *The London, Edinburgh, and Dublin philosophical magazine and journal of science*, vol. 2, no. 11, pp. 559–572, 1901.

- [3] C. Zong, J. Xu, J. Song, S. Xin, S. Chen, W. Wang, and C. Tu, "P2m: A fast solver for querying distance from point to mesh surface," *ACM Transactions on Graphics (TOG)*, pp. 1–11, 2023.
- [4] M. P. Corso, F. L. Perez, S. F. Stefanon, K.-C. Yow, R. García Ovejero, and V. R. Q. Leithardt, "Classification of contaminated insulators using k-nearest neighbors based on computer vision," *Computers*, vol. 10, no. 9, p. 112, 2021.
- [5] T. Liu, C. Rosenberg, and H. A. Rowley, "Clustering billions of images with large scale nearest neighbor search," in *2007 IEEE workshop on applications of computer vision (WACV'07)*. IEEE, 2007, pp. 28–28.
- [6] P. Quin, G. Paul, and D. Liu, "Experimental evaluation of nearest neighbor exploration approach in field environments," *IEEE Transactions on Automation Science and Engineering*, vol. 14, no. 2, pp. 869–880, 2017.
- [7] J. L. Bentley, "Multidimensional binary search trees used for associative searching," *Commun. ACM*, vol. 18, no. 9, p. 509–517, sep 1975. [Online]. Available: <https://doi.org/10.1145/361002.361007>
- [8] A. Guttman, "R-trees: a dynamic index structure for spatial searching," in *Proceedings of the 1984 ACM SIGMOD International Conference on Management of Data*, ser. SIGMOD '84. New York, NY, USA: Association for Computing Machinery, 1984, p. 47–57. [Online]. Available: <https://doi.org/10.1145/602259.602266>
- [9] A. Rodriguez and A. Laio, "Clustering by fast search and find of density peaks," *science*, vol. 344, no. 6191, pp. 1492–1496, 2014.
- [10] M. Muja and D. G. Lowe, "Scalable nearest neighbor algorithms for high dimensional data," *IEEE Transactions on Pattern Analysis and Machine Intelligence*, vol. 36, no. 11, pp. 2227–2240, 2014.
- [11] N. Wang, B. Wang, W. Wang, and X. Guo, "Computing medial axis transform with feature preservation via restricted power diagram," *ACM Transactions on Graphics (Proc. SIGGRAPH Asia)*, vol. 41, no. 6, pp. 1–18, 2022.
- [12] A. Bowyer, "Computing Dirichlet tessellations\*," *The Computer Journal*, vol. 24, no. 2, pp. 162–166, 01 1981.
- [13] H. Si, "Tetgen, a delaunay-based quality tetrahedral mesh generator," *ACM Trans. Math. Softw.*, vol. 41, no. 2, feb 2015. [Online]. Available: <https://doi.org/10.1145/2629697>
- [14] S. Hert and M. Seel, "dD convex hulls and delaunay triangulations," in *CGAL User and Reference Manual*, 5.6.1 ed. CGAL Editorial Board, 2024. [Online]. Available: <https://doc.cgal.org/5.6.1/Manual/packages.html#PkgConvexHullD>
- [15] G. Voronoi, "Nouvelles applications des paramètres continus à la théorie des formes quadratiques. premier mémoire. sur quelques propriétés des formes quadratiques positives parfaites," *Journal für die reine und angewandte Mathematik (Crelles Journal)*, vol. 1908, no. 133, pp. 97–102, 1908. [Online]. Available: <https://doi.org/10.1515/crll.1908.133.97>
- [16] K. L. Cheung and A. W.-C. Fu, "Enhanced nearest neighbour search on the r-tree," *SIGMOD Rec.*, vol. 27, no. 3, p. 16–21, sep 1998. [Online]. Available: <https://doi.org/10.1145/290593.290596>
- [17] A. Papadopoulos and Y. Manolopoulos, "Performance of nearest neighbor queries in r-trees," in *Database Theory — ICDT '97*, F. Afrati and P. Kolaitis, Eds. Berlin, Heidelberg: Springer Berlin Heidelberg, 1997, pp. 394–408.
- [18] J. McNames, "A fast nearest-neighbor algorithm based on a principal axis search tree," *IEEE Transactions on Pattern Analysis and Machine Intelligence*, vol. 23, no. 9, pp. 964–976, 2001.
- [19] Y. A. Malkov and D. A. Yashunin, "Efficient and robust approximate nearest neighbor search using hierarchical navigable small world graphs," *IEEE Trans. Pattern Anal. Mach. Intell.*, vol. 42, no. 4, p. 824–836, apr 2020. [Online]. Available: <https://doi.org/10.1109/TPAMI.2018.2889473>
- [20] J. L. Blanco and P. K. Rai, "nanoflann: a C++ header-only fork of FLANN, a library for nearest neighbor (NN) with kd-trees," <https://github.com/jlblancoc/nanoflann>, 2014.
- [21] J. Vermeulen, A. Hillebrand, and R. Geraerts, "A comparative study of k -nearest neighbour techniques in crowd simulation," *Computer Animation and Virtual Worlds*, vol. 28, p. e1775, 05 2017.
- [22] Boost, "Boost C++ Libraries," <http://www.boost.org/>, 2015, last accessed 2015-06-30.
- [23] Q. Zhou and A. Jacobson, "Thing10k: A dataset of 10,000 3d-printing models," *arXiv preprint arXiv:1605.04797*, 2016.
- [24] S. Koch, A. Matveev, Z. Jiang, F. Williams, A. Artemov, E. Burnaev, M. Alexa, D. Zorin, and D. Panozzo, "Abc: A big cad model dataset for geometric deep learning," in *The IEEE Conference on Computer Vision and Pattern Recognition (CVPR)*, June 2019.
- [25] C. R. Qi, L. Yi, H. Su, and L. J. Guibas, "Pointnet++: Deep hierarchical feature learning on point sets in a metric space," *CoRR*, vol. abs/1706.02413, 2017. [Online]. Available: <http://arxiv.org/abs/1706.02413>
- [26] J. Li, J. Zhou, Y. Xiong, X. Chen, and C. Chakrabarti, "An adjustable farthest point sampling method for approximately-sorted point cloud data," in *2022 IEEE Workshop on Signal Processing Systems (SiPS)*, 2022, pp. 1–6.